5-2020

Carbonaceous Nanomaterial: Rapid Synthesis, Property Characterization and Theoretical Analysis

Varun Gupta
The University of Texas Rio Grande Valley

CARBONACEOUS NANOMATERIAL: RAPID SYNTHESIS, PROPERTY CHARACTERIZATION AND THEORETICAL ANALYSIS

A Thesis

by

VARUN GUPTA

Submitted to the Graduate College of
The University of Texas Rio Grande Valley
In partial fulfillment of the requirements for the degree of

MASTER OF SCIENCE IN ENGINEERING

May 2020

Major Subject: ELECTRICAL ENGINEERING

CARBONACEOUS NANOMATERIAL: RAPID SYNTHESIS, PROPERTY CHARACTERIZATION AND THEORETICAL ANALYSIS

A Thesis
by
VARUN GUPTA

COMMITTEE MEMBERS

Dr. Samir Iqbal
Chair of Committee

Dr. Nazmul Islam
Committee Member

Dr. Laura Benitez
Committee Member

May 2020

ABSTRACT

Gupta, Varun, Carbonaceous Nanomaterial: Rapid Synthesis, Property Characterization And Theoretical Analysis. Master of Science (MS), May, 2020, 41 pp., 10 figures, 40 references.

In this thesis, An environmentally friendly and rapid synthesis of highly porous carbon nanomaterial is presented. The direct pyrolysis of the cane sugar was achieved in a hand-fabricated Teflon microchamber. Homogeneous heating and quick pyrolysis were carried out in 3 minutes using a household microwave oven. The porosity and surface area enhancement is obtained by in-step decompositions of household baking soda (sodium bicarbonate), a common household chemical. Sodium bicarbonate was specifically used to impregnate porous carbon foam with sodium oxide nanocomplexes, which were later washed to improve surface area and reduce oxygen content, making it suitable for applications such as battery anode. The ill effects of presence of oxygen based impurities in anode carbon material on intercalated alkali ions was analyzed by Density Functional Theory simulations. The surface properties, elemental composition and crystallinity of the material were analyzed with field emission scanning electron microscope (FESEM), energy dispersive x-ray spectroscopy (EDS) and x-ray diffraction (XRD) data. The data showed in step development of carbon material into high surface area carbon nanosphere morphologies with reducing oxygen content due to decomposition of sodium bicarbonate.

DEDICATION

The completion of my master's studies would not have been possible without the love and support of my family. I would like to dedicate my thesis to my mother Dr. Mridul Gupta and my sister, Mansi who wholeheartedly inspired, motivated and supported me to accomplish this degree. Thank you for your love and patience.

ACKNOWLEDGEMENTS

I will always be grateful to Dr. Samir Iqbal, chair of my dissertation committee, for all his mentoring and advice. He encouraged me to complete this process through his infinite patience and guidance. My many thanks to my co-advisor: Dr. Nazmul Islam, who gave me his valuable guidance during my entire degree and helped me every time I was in need. I would also like to thanks my committee member:Dr.Laura Benitez, who helped me to complete significant parts of this thesis and accepted to guide me through theoretical analysis. All of their advice, input, and comments on my dissertation helped to ensure the quality of my intellectual work.

The authors acknowledge the Texas Advanced Computing Center (TACC) at The University of Texas at Austin for providing {HPC, visualization, database, or grid} resources that have contributed to the research results reported within this thesis.

I would also like to thank my Graduate College at UTRGV to make me financially stable by providing Presidential Graduate Research Assistantship. I would also like to thank all my friends at NanoBio Lab in UTRGV.

TABLE OF CONTENTS

Page

LIST OF FIGURES

Page

CHAPTER I

INTRODUCTION

The trend in the world is turning towards the green energy. Renewable energy generation have started to replace a big proportion of the conventional energy in the energy production statistics. TheNatural sources such as solar and wind have become increasingly popular, their characteristic irregular energy generation due to unpredictable factors would require efficient energy storage technology for distribution to energy grids when needed.Electric vehicles are expected and intended to play an important role for future mobility scenarios because they are compatible with the worldwide need for effective CO2 savings in combination with the enhanced usage of renewable electric energy coming from wind, water and solar power plants. The future of our world will be defined by new advents in electric-powered transportation and renewable energy distribution and we are headed rapidly towards a major paradigm shift. Therefore, energy storage is more important today than anytime in human history.

Lithium (Li) ion batteries (LIBs) have dominated the past decade in the energy storage and is a candidate for the possible solution towards the green energy revolution. Li is the lightest metallic ion and have very low redox potential (-3.0V) [1] between Li metal and Li^+ ion, which results into very high battery potential. The size of Li^+ ion is very small which makes it ideal for intercalation and deintercalation into nano porous structures during charging/discharging. Small size also means low diffusion coefficient for the ion which assists in easy ion conduction in electrolyte. Combining Li ion chemistry with long cycle life, it is expected to continue to

dominate the energy storage industry for long [2-3]. With the possibility of rise in global demand, there will be increase in prices. Many global lithium reserves are also located in remote or in politically sensitive areas [4]. Due to limited Li ion resources and consequent expected price rise, sodium ion batteries (NIBs) will pose as a possible alternative [1]. Sodium is abundantly available hence cheap, have similar redox potential as lithium (only 0.3V lower) so high battery potential [1] and is omnipresent, therefore environment friendly.

Carbon being the anode material in the LIBs & NIBs, efforts have been made to find the best possible host structure. Lithium and Sodium metal are being studied as the anode materials for Li-ion and Na-ion batteries, respectively. Lithium metal is considered to be an ideal anode material for Li-ion rechargeable batteries due to its extremely high theoretical specific capacity (3860 mA h g^{-1}), low density (0.59 g cm^{-3}) and the lowest negative electrochemical potential (−3.040 V *vs.* the standard hydrogen electrode)[29]. Unfortunately, uncontrollable dendritic Li growth and limited Coulombic efficiency during Li deposition/stripping inherent in these batteries have prevented their practical applications over the past 40 years[29]. Sodium metal also presents itself as a ideal anode material for the Na ion rechargable battery with high theoretical capacity (1166 mA h g^{-1})[30] and easily available abundant resources. Several factors hinder the applicability of Na metal anodes in future larger scale, such as unstable solid electrolyte interphase, large volume change upon cycling and safety concerns related to the uncontrolled dendritic Na growth[31].

Materials such as carbon nano tubes [5-7], reduced graphene oxide [8-9]& graphene [10] itself have attracted huge attraction for energy storage purposes but the synthesis procedures of these materials is quite complex (CVD, mechanical exfoliation)[11-13] and need strict experimental conditions [13]. These processes being complicated and time consuming has in turn inhibited the wide growth of energy storage industry. For a sustainable global green energy revolution, we need materials which are simple to synthesize, doesn't require adverse initial chemical reactants such as greenhouse gases (Methane[11]), are green and cost effective.

Here we are introducing a carbon foam like material which is quick and easy to synthesis, environment friendly, inexpensive since reactants are only cane sugar and baking soda, and could be employed in a battery as well as supercapacitor electrode. These properties make it ideal as an industry material for large scale production to grow energy storage in a sustainable way.

Porous carbon foams have been a material of interest as low-cost high-performance energy storage materials [14-18]. Strubel, et. al [18] made a carbon foam using Zinc oxide nanoparticle hard template along with sucrose as a precursor, which yielded impressive results. But this work was quickly superseded by an ingenious method by Wang, et. al.[19] where they were able to pyrolyze sucrose without the use of any hard template. Wang's method was facile using Zinc Nitrate decomposition releasing NO_2 gas during synthesis of carbon material inducing porosity. Although this method was fast compared to other methods, there still lies a scope to reduce the synthesis time from hours to minutes while enhancing surface area/porosity multifold.

We explored that the pyrolysis treatment of sucrose can be expedited under the hydrothermal conditions. Rana, et. al.[20] reduced the time for hydrothermal synthesis of the ZnO nanostructures from 2 hours to 5 minutes by using domestic microwave oven and we followed the same procedure to grow our carbon material.

CHAPTER II

MOTIVATION

We took motivation from Rana, et. al. [20]'s microwave technique to accelerate and simplify the hydrothermal carbonization by pyrolysis of cane sugar done by Wang, et. al [19], along with enhancing porosity by introducing household baking soda in the precursor solution.

Compared to conventional heat transfer to the material by convention, conduction or radiation, heat energy can be much more uniformly/efficiently applied when it is derived from the material's molecular interactions. Since the heat required for reaction is directly supplied or induced from the reactants, it reduces the energy wasted in conduction/absorption by container mediums while reducing synthesis time significantly. Hence the microwave treatment is the key for an efficient hydrothermal carbon synthesis.

2.1 Hydrothermal Synthesis

Hydrothermal synthesis refers to a reaction involving reactants being components of two or more phases (heterogeneous reaction), one of the component phase being water, taking place above 100ºC and 1 bar pressure [34]. In simple language, we can break the term hydro (water) + thermal (heating) or heating your reactants in water at very high temperature and pressure. Several minerals in nature form under these circumstances. Geologists and mineralogists have been able to determine the conditions required for this synthesis which are now employed in many industries, such as hydrometallurgy: classic Bayer's process for decomposition of bauxite ore.

The hydrothermal method is a low cost, environmentally friendly technique which can be used on large area and/or flexible substrates, as well as fabrication of free standing nanostructures and hence is of considerable interest for practical applications. The growth of different nanostructures in this process depends mainly on the growth temperature, precursors used, addition of surfactants or other chemicals for modifying the nanostructure growth, solution pH value, crystal properties of the material, as well as substrate type and pretreatment (such as deposition of seed layer).

One of the very important issue in this synthesis process is to achieve specific dimensions of the nanostructures to obtain the maximum possible surface area. In our process we have added the sodium bicarbonate in the reactants during pyrolysis of the cane sugar to obtain the maximization of surface area in the shortest time possible as discussed in further sections.

2.2 Microwave Treatment

Rapid heating under microwave irradiation was achieved via the dipolar polarization of water molecules. Irradiation raises the temperature of the whole solution simultaneously which accelerates the reaction and crystallization. In the proposed microwave-assisted hydrothermal method, water is used as a dipolar solvent and heat is produced by the rotation, friction, and collision of water molecules under the influence of a rapidly changing alternating electric field from the oven. Furthermore, the dissolved ions in the solution move constantly under the influence of the fluctuating electric field (microwaves), causing a sharp increase in the local temperature of the ions due to friction and collision [21].

2.3 Special Fabricated TEFLON VESSEL

Besides rapid heating, another important factor in microwave-assisted hydrothermal methods is the existence of a pressurized environment inside the reaction vessel. An autoclave is the common choice for reaction vessel for conventional hydrothermal synthesis. We fabricated a teflon microchamber from a teflon rod bought from Amazon as shown in Figure 2.1, with the dimension as 3.5 cm inner diameter and 6 cm inner height with a volume of around 60ml.

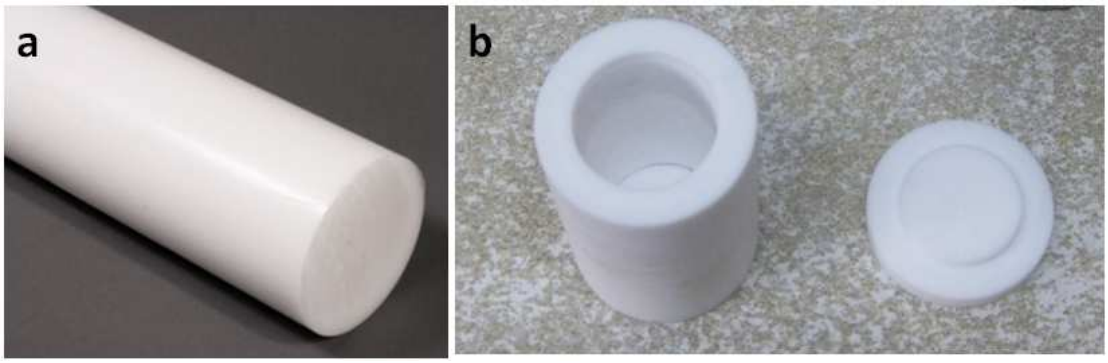

Figure 2.1 (a) Teflon rod bought from Amazon and (b) the closed reaction vessel fabricated from the rod.

Teflon or Poly Tetra Fluoro Ethylene was used the building material for this vessel as it is transparent to microwaves since it isn't a polar molecule. To avoid the rapid evaporation of the solution under high power microwaves, we use a closed reaction system rather than an open reaction system. The closed reaction system facilitates pressurized conditions that could raise the temperature of a solution well above its boiling point. Hence, the ultrafast chemical reactions are not only because of the elevated temperature, but also due to the pressurized conditions inside the vessel. The whole process is very sensitive, because any extra pressure created inside the

sealed vessel could burst it with devastating results. To manage this extra pressure, Rana, et. al. made a small hole in their 300ml vessel (Figure 2.2 Ref. [20]), which continuously relievessome pressure to safely maintain certain value of high pressure inside the vessel.

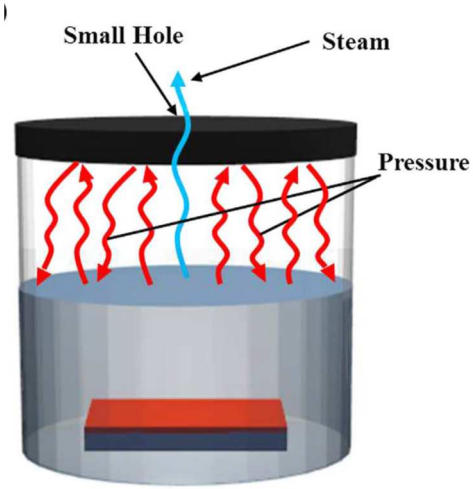

Figure 2.2 Vessel used by Rana, et. al for synthesis of ZnO nanostructures. Image reference [20].

The heating of a solution by microwaves also depends on its volume and the depth. The penetration depth is the point at which 37% of the initially irradiated microwave power exists effectively in the solution[32]. The penetration depth of 2.45 GHz microwaves in water is 5 cm at 100 °C[32]. If the volume and depth of the solution is above5 cm, the remaining solution will be heated via convection rather than irradiation, which could alter the composition of the material acquired at the end. Hence, we chose the dimensions of our teflon vessel to be of the range of 5 cmso area of the solution was homogeneously exposed to the microwave radiation.

Baking soda or Sodium Bicarbonate ($NaHCO_3$) decomposition on heating emits water vapours (H_2O) at lower temperatures and carbon dioxide (CO_2) gas at elevated temperatures (500-600ºC) (equation (1)). During synthesis of the carbon structure its decomposition inflates the carbon like flour dough inflates while baking bread. $NaHCO_3$ also plays a crucial role in reducing the carbon's oxygen content, which is one of the causes of cation deposition in the anode (carbon) after intercalation. Highly electropositive cations (Li^+/Na^+) reacts with oxygen content in the anode to form the metal oxides and tend to an irreversible deposit since metal oxides have higher formation energy than the metal itself. The carbonic acid (H_2CO_3) reduce the oxygen bonding within the carbon structure [22] giving out water and Na salt (equation (2)).

$$2NaHCO_3 \rightarrow Na_2CO_3 + H_2O\uparrow + CO_2\uparrow \qquad (1)$$

$$NaHCO_3 + H_2O \leftrightarrow Na^+ + H_2CO_3 + OH^- \qquad (2)$$

.

CHAPTER III

SYNTHESIS AND ANALYSIS

3.1 Setting up the Standard Synthesis Procedure

We tried many compositions and microwave exposure time to find the standard procedure to fabricate our material, mainly because we did this our specially fabricated vessel. It was important to do this to figure out the effect of combinations of reaction concentration and microwave exposure time on the shape and size of nanostructures. To set-up the standard procedure, Zinc Oxide (ZnO) nanostructures were fabricated using different compositions of molarities of reactant solutions of Hexamethyl-tetramine or Methanamine (50mM) and Zinc Nitrate hexahydrate (50mM). On Si substrate a seed layer was formed for each sample by drop casting 22mM solution of Zinc acetate in de-ionised water for the nucleation of growth. ZnO was chosen because it is widely synthesized using hydrothermal process and there were ample micrographs published to compare our figures below.

Morphologies in- figure 3.1 a) was synthesized by 1:1 ratio of 25mM methanamine and 75mM $ZnNO_3.6H_2O$ exposed for 2min to microwave, figure 3.1 b) was synthesized by 1:1 ratio of 50mM methanamine and 50mM $ZnNO_3.6H_2O$ exposed for 3minutes to microwaves and for figure 3.1 c) and d) was synthesized by 1:1 ratio of 50mM methanamine and 50mM

$ZnNO_3.6H_2O$ exposed to microwave for 5 and 7 minutes respectively. Figure 3.1 e) is a zoomed version of figure 3.1 d) to show the sharp structures synthesized by this method.

Similar test runs were done for our Carbon material to find the most appropriate set of conditions and circumstances. In the following section the final combination of microwave exposure, concentration, ratio of precursors, pretreatment of substrate and other experimental conditions are discussed for a convenient synthesis of final product.

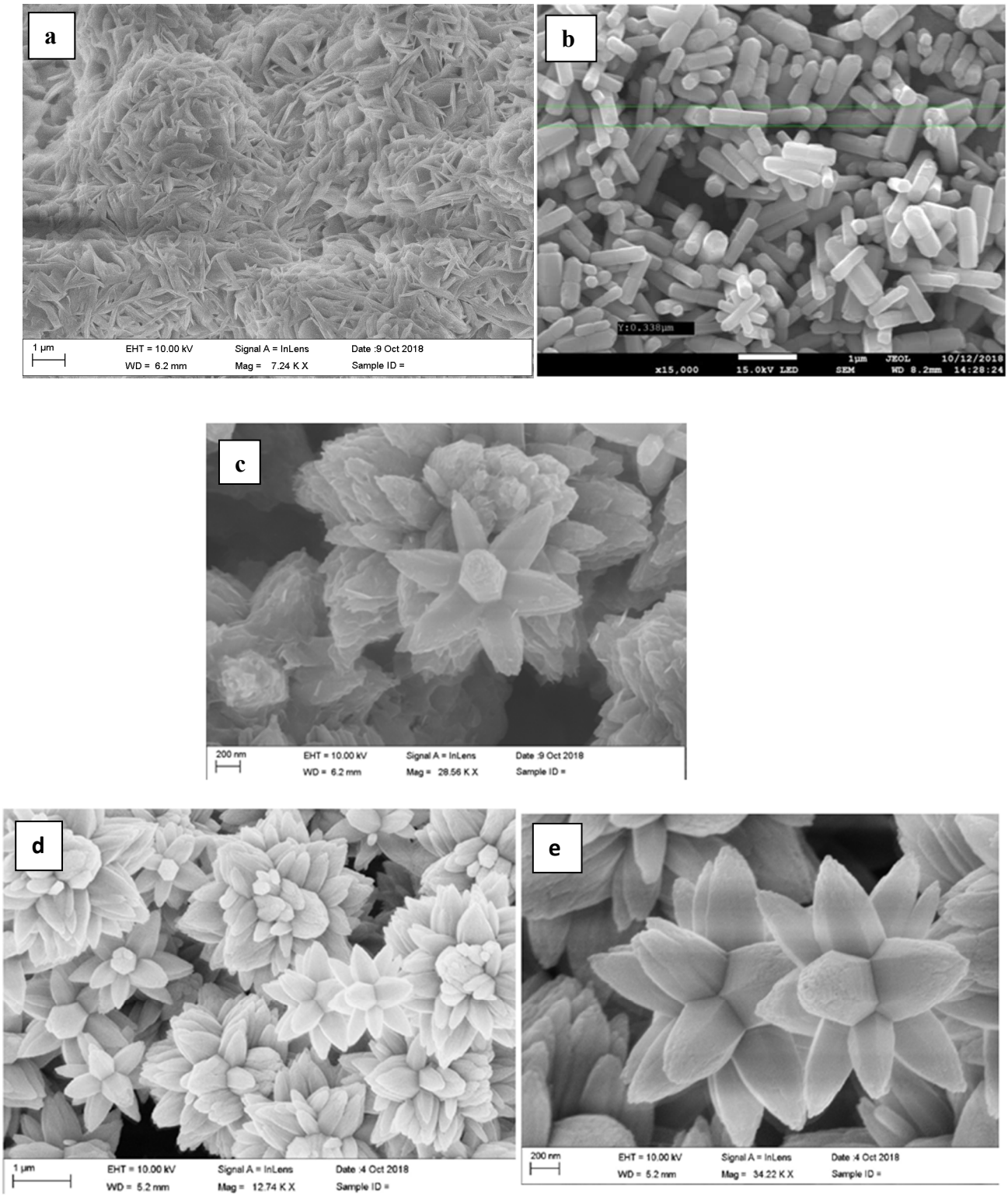

Figure 3.1 ZnO nanoflower morphologies obtained while trying different combinations of ratios of reactant solutions. See text for details.

3.2 **Standard Synthesis Procedure of our Carbon Material in Steps**

We took 30ml of precursor solution of 4g of equal weight ratio of cane sugar ($C_6H_{22}O_{11}$) and sodium bicarbonate in deionised water, in a homemade 60ml Teflon microchamber. This Teflon container was sealed by the Gorilla tape in such a way that it'll hold the cap but let any extra pressure leak to avoid explosions. The Teflon vessel was exposed to a domestic countertop microwave oven at maximum power of 900 Watts for 3 minutes (step 1). The base of the oven we used rotates at the rate of 4 rounds per minute which further assists the homogeneous heating by the microwaves. Black foam like chunk of solid was obtained as product which was further annealed in N_2 gas inert environment at 800 ℃ for 5 hours (step 2) for further decomposition of sodium carbonate into sodium oxide and CO_2, further inflating the foam. The obtained product was washed multiple time with DI water to wash away the soluble sodium oxides or other sodium complexes (step 3). For further possible deoxygenation of the sample, we sonicated the sample in a pH 9 solution of NaOH added with 2g of $NaHCO_3$. The solution was heated at 90 ℃ for 3 hrs. Sample was extracted by centrifuge and washed with DI water several times (step 4).

3.3 Characterization and Analysis Techniques Used

Obtained samples were analysed by X-ray diffraction using set-up Bruker Phaser-2, for crystallographic evolution at each step. The surface morphology was explored by Field Emmision Scanning Electron Microscope (FESEM)done on Carl Zeiss, Sigma VP microscope and elemental composition analysis was done by the energy dispersive spectroscopy analysis (Octane Super EDS system). Fourier Transform Infrared Analysis was also done to analyze the composition of the bonds present in the material as impurity.

CHAPTER IV

RESULTS AND DISCUSSIONS OF EXPERIMENTS

FESEM analysis of our final products (Fig. 4.1(a)) post step-3 shows the range of nano filament/sphere dia we can have i.e. 100nm-200nm. Since it is a template free hydrothermal synthesis, the size of the nanostructures depends on the amount of pressure and heat supplied. The size of the nanosphere in Fig. 4.1(b), 0.8μm in diameter, was obtained by a longer microwave treatment time and lower power setting of 700W.

Though the smaller structure is preferred for high surface area to volume ratio for intercalation/deintercalation. Hence morphology after the step-3 would work best for energy storage applications. The X-ray diffraction pattern was observed to show the consistency of the process occurring as intended at each step. It can be traced with the XRD pattern that the sodium bicarbonate added in the precursor is breaking down. Post step-1 XRD analysis (Fig. 4.2 (a)) shows the characteristic peaks of the sodium carbonate, hence the reaction in equation (1) is taking place after the microwave treatment of the baking powder along with the sugar. Here during the pyrolysis of sugar into the carbon, the sodium carbonate particles are also being created. The importance of the microwave treatment can be appreciated as the heating process of the reactants dissolved in solution is homogenous and so will be decomposition of the sodium bicarbonate into sodium carbonate. Hence the distribution of these sodium carbonate particles in the carbon foam generated will be homogeneous even after the rapid heating. These carbonate particles will be ingrained all over in the carbon chunk obtained as the first product. Step-2

focuses to decompose the Na2CO3 even further to release CO2 gas to make the carbon foam more porous and enhance surface area.

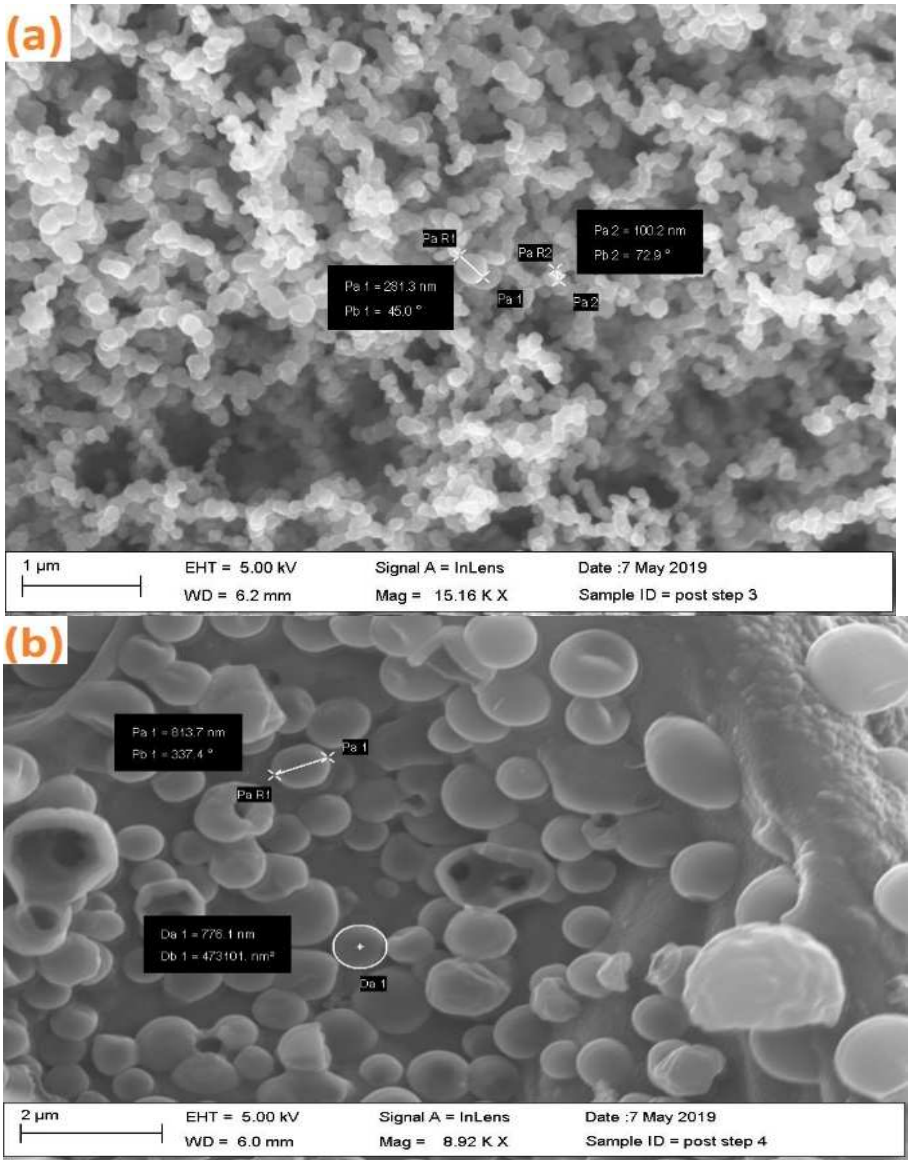

Figure 4.1 FESEM micrographs of the final products after step-3 (a) and step-4 (b).

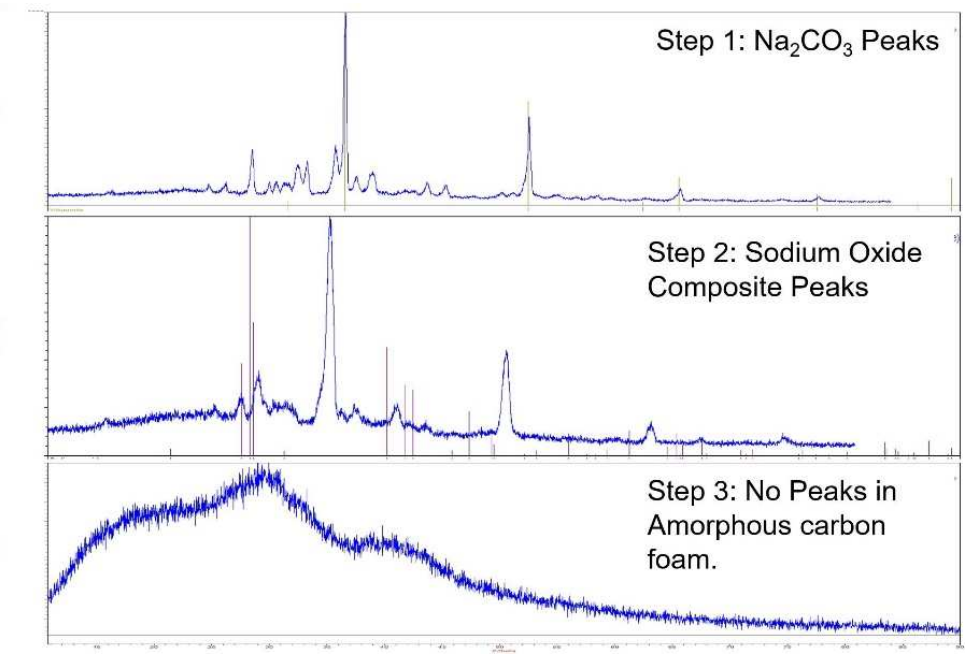

Figure 4.2 XRD analysis tracking the crystallinity of the carbon foam at each step. Post step 1 (a) peaks of sodium carbonate, post step 2 (b) peaks of mixed oxides and carbonate and post step 3 (c) No distinct sharp peaks showing amorphic character of the final product.

The peaks in XRD of step-2 doesn't resemble to any one of the sodium oxides (Na2O, Na2O2 or NaO) so the crystal inside can be a composite of sodium oxides and remains of some carbonates from the last step. Step 2 though is not necessary and was only performed to certain the decomposition of the Na2CO3. The size of sodium bicarbonate particles is larger than the sodium oxide particles and hence when it is washed away in step 3, the surface area enhanced will be comparable to the product obtained with step 2 included in synthesis. Hence this step can be bypassed for large scale industry manufacturing and reducing the time and resources for synthesis significantly. Step-3 washes away all the present Na composites (oxides/salts) leaving behind the pores which would enhancing the surface area. The XRD post step-3 shows no

specific sharp peaks which means that the sample is amorphous now and supports our claim of salts being washed away, leaving behind our final carbon product.

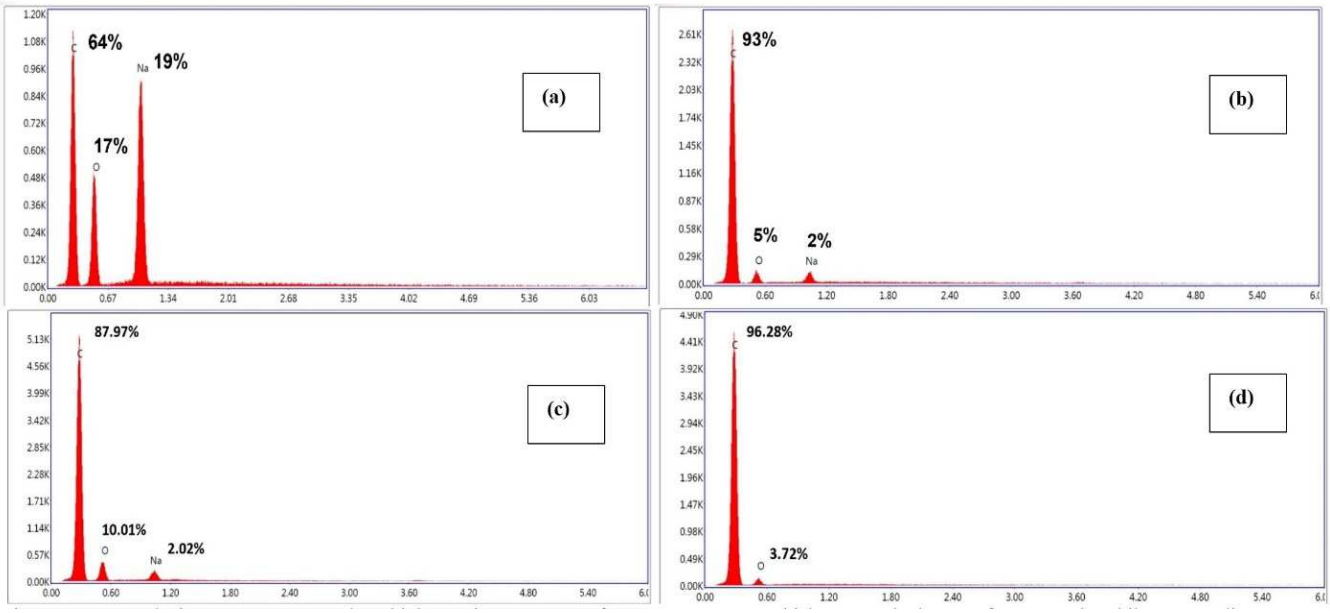

Figure 4.3 EDS analysis post step-2 (a) to show high atomic percentage of Na atom presence, which was washed away after step 3 (b) while some sodium composite remained as impurity. Step 4 was aimed to further reduce the oxygen content but post step 4 (c) number of oxygen atoms went up. EDS of commercial GNTS (d) for comparison.

Energy dispersive X-ray spectroscopy (EDS) is also done to do the elemental analysis and check for the purity of the sample. In battery application, the presence of oxygen in the anode material inhibits the performance as discussed in previous sections. Thereby the aim was to reduce the oxygen content as much as possible and that's why the deoxygenation of step-4 was included in synthesis. The EDS analysis however shows that after the further treatment in step 4, the atomic weight percentage (atm. wt. %) of oxygen atoms increased (Fig 4.3 (c)) hence not recommended for final product synthesis. After step-3, the atomic percentage of the oxygen in our sample (5.74%, Fig. 4.3 (b)) was as compared to the pristine Graphene Nanoplatelets

(GNTs) (3.72%, Fig. 4.3 (d)) (ALDRICH chemicals, grade C-750) which are explored as anode material in earlier research [23-25].

The reason for the oxygen content in the pristine GNTs is the binding of the atmospheric or aerial oxygen by weak van der Waals interactions [27]. Our sample's oxygen content could be because of the aerial oxygen binding as well as inefficient removal of the deep ingrained Na complexes as trace quantities might be trapped in the carbon structure. Hence, we conclude that there is no need for further deoxygenation treatment for the sample post step 3. Also, comparison of the sample after the microwave treatment (step-1) and step-3 shows that the baking soda excellently worked as the reducing agent since the oxygen content noticeably reduced from 23.11% (Fig. 4.2 (a)) to 5.74% in (Fig. 4.2 (b)).

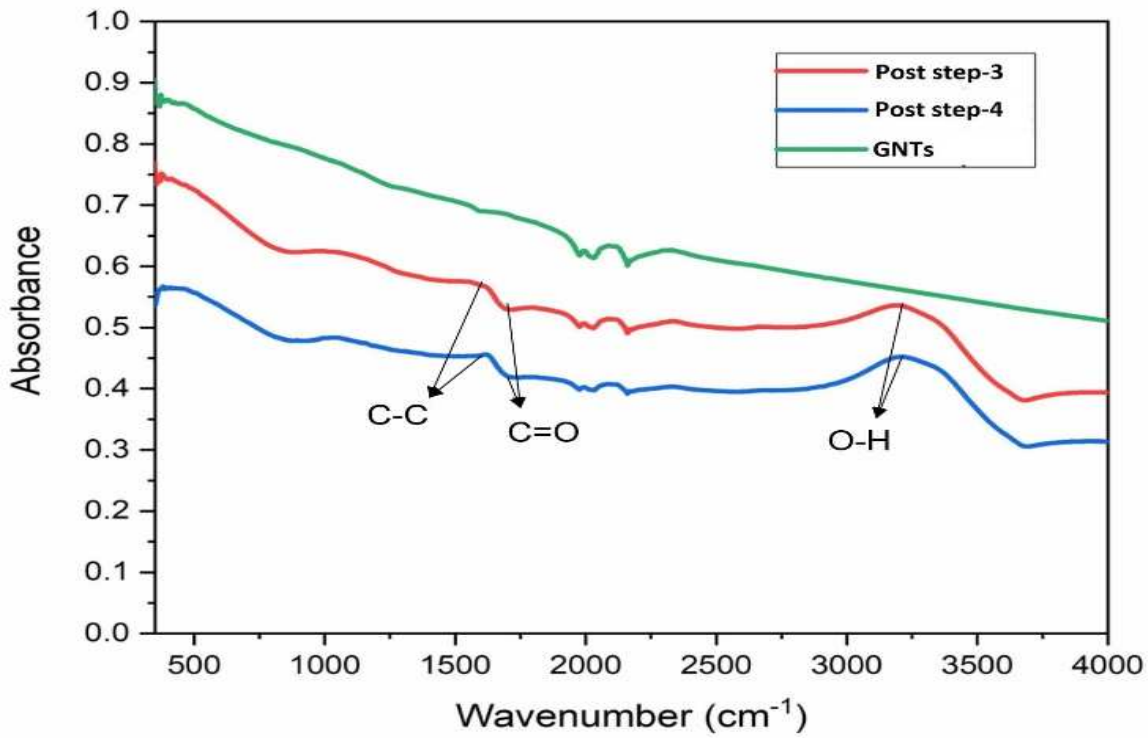

Figure 4.4 FTIR analysis showing the oxygen related groups present in the sample. As post step-3 and step-4 spectra are same, indicating no further reaction occurring in step-4.

After getting the elemental quantitative analysis, we did Fourier Transform Infrared Spectroscopy to do the qualitative analysis and identify oxygen related group frequencies present. This measurement investigated the form in which oxygen was present as impurity. Fig 4.4 shows a comparison between the FTIR analysis of our samples and the commercial GNTs. The broad and weak peak of our sample at ~3250 cm-1 after step-3&4 is ascribed to the hydroxyl group (OH) stretching [28]. This is one of the sources of the oxygen content shown in EDS analysis. Hydroxyl stretching could have resulted from water vapour trapped in our sample, but it is not shown in the commercial sample peaks (Fig.4.4 Green). Our explanation to this is the trapping of the ambient water vapours in the pores of our high surface area sample. The small/weak peak observed at 1620 cm-1 can be attributing to the resonance C-C stretching and adsorbed hydroxyl group [29]. Similar small peak at 1720 cm-1 indicates C=O bonding [29] which is present in the carbonate ion of the sodium carbonate, and could be present in traces as impurity, as also concluded in EDAX analysis. Since any specific/large peaks were not observed corresponding to the carbon oxygen bond, we can clearly conclude that the major oxygen content in our sample is trapped in the form of impurity (sodium complexes) and ambient water/oxygen.

In our carbon material, inevitable oxygen is trapped mainly as sodium complex and negligible other impurities. Hence when it is employed as an anode in sodium ion battery, the ions will not be oxidizing when intercalating for charging since nothing to react with. This process of pre-sodiation will therefore basically be assisting in efficient working of the sodium ion battery or even supercapacitors where the intercalation/deintercalation process is rapid. The size of the Na+ and Li+ is 1.02 Å26] and 0.76 Å[26], which are smaller than any of the sodium complex particles. Since the porosity of our sample will be of the range of the sodium complexes washed away in step 3, our sample material will be quite suitable for the Na or Li ion energy

storage application. To be employed as the energy storage material, we would only need to follow up to synthesis step 3. Step 2 can also be skipped for fast industry product in 3 minutes; however, this will be compromising the surface area. Overall, eco-friendly precursors and the quick & facile synthesis technique make it ideal for large scale industry application.

CHAPTER V

THEORETICAL ASPECTS: DFT ANALYSIS

5.1 Introduction: Simulation Review

It is critical to appreciate the elemental relationship between the atomic structure and chemical as well as physical properties. Density functional theory (DFT) and, in particular, the B3LYP hybrid density functional theory is widely applied in molecular modelling studies to predict and display structures, spectroscopic parameters and energy changes of small, middle and large size molecules in chemistry [34]. The fruitful combination of theoretical calculations and practical results permits profound understanding of the research problem and better insight of the phenomena under investigation.

Density functional theory calculations for optimization of system simulation of 6x6 graphene layer, acting as an anode and intercalated Li^+/Na^+ ion were done to find its lowest possible energy configuration. Simulations were exercised by using Gaussian G16 software [35] at the level of B3LYP with a basis set of 3-21G or 6-31G, which adopts a fully self-consistent density functional calculation by solving the standard Kohn–Sham equations. To understand this properly, let's discuss some basics.

5.2 Background of Density Functional Theory (DFT)

Understanding the configuration and properties of materials has been the interest of physicists and chemists since always. One way they explain the material system is by defining the Hamiltonian of the system under consideration, and then solving the Schrödinger's equation for that Hamiltonian exactly. Well, sounds like they just have to solve an equation, what's the catch? The catch is to solve it exactly.

Solving the Schrödinger's equation for a system (e.g. electron gas) with the Hamiltonian containing many complex terms (like exchange-correlation function, electron-electron interaction potentials) is a formidable, difficult and sometimes near impossible task. Hence to make system/problem simpler, we scientists make some approximations for the system and get an approximate but close solution for the problem. Prominent task of the scientists is to make an approximation that doesn't compromise the actual system too much.

I have used one such famous and interesting approximation called the Density Functional Theory (DFT) to solve the system defining Kohn-Sham equations. Kohn–Sham equation is the one electron Schrödinger equation of a fictitious system of non-interacting particles that generate the same density as any given system of interacting particles. In DFT, the energy which is obtained by the wave function is rather defined as a functional of electron density than its variables, hence the name. The wave function for a N particle system in 3 dimensions, is a vector containing 3N variables (only spatial consideration) and that can make computation too much of labor. If we can calculate energy by only estimating only electron density, things ease up. DFT is a very good approximation to find the ground state energy.

The major issue in solving the Hamiltonian equation is the electron-electron interaction. Due to the fast motion of the electrons, the position dependent coulombic potential changes rapidly and is hard to predict the interaction energy. Kohn-Sham suggested to alter the problem by considering the electron's in the system to be non-interacting with each other. In that sense, the interaction among electron's was decomposed into: Coulombic, exchange and correlation interactions. Coulombic interactions were addressed by Hartree-Fock approximation, which considers that each electron is interacting with a general local potential defined by the density of all electrons. Exchange and correlation interactions are further complicated to formulate for a system and to understand this, one must know what exchange and correlation energies mean.

Exchange energy is the quantum contribution to the total energy, due to spin of the electrons. Electrons as fermions follow the Pauli's exclusion principle, i.e. two electrons cannot possess same quantum state. This means when two electrons with same spin try to come close to each other spatially, along with coulombic force they face quantum degeneracy pressure as repulsion. This produces a spatial separation between electrons with same spin and thus reduces the coulombic energy of the electronic system. This reduction in energy due to same spin of the identical electrons is called exchange energy.

Correlation energy is the quantum contribution due to the opposite spin of the electrons. As the similar spin favors the spatial difference between electrons, opposite spin favours them to come close. This will increase the coulombic energy and Kinetic energies of the electrons increases so that they go farther from each other. This energy for a complex system is extremely complicated to calculate. No present method is tractable in total energy calculation at any degree of complexity.

Density functional theory gives some hope of a simple method of describing the exchange and correlation energies. The theory says that the total energy including exchange and correlation energies of an electron gas is a unique functional of the electron density. The minimum value of the total energy functional is the ground state energy ($E[\rho_{ground\ state}]$) of the system, and the density that yields this minimum value is the exact single-particle-ground-state density. i.e. if ρ_0 is not the ground state density of the system, then $E[\rho_0] > E[\rho_{ground\ state}]$.

With approximation for electron-electron interaction such as Hartree Fock and for exchange-correlation, transformed one electron Schrödinger equation of a fictitious system of non-interacting particles that generate the same density as any given system of interacting particles is obtained.

B3LYP Hybrid Potential

Becke3-Lee-Yang-Parr [36] is used to approximate the complicated electron-electron interactions. This functional is a hybrid of exact (Hartree-Fock) exchange with local and gradient corrected exchange terms in combination of correlation approximated by LYP [36]. The approach to construct a hybrid potential to estimate better approximations of electon-electron interaction was first introduced by Axel Becke in 1993 [37]. Hybridization provides simple scheme to closely approximate the molecular properties.

5.3 What we have done

We have used Gaussian G16 software [35] at the level of B3LYP with a basis set of 3-21G and 6-31G to first optimize the structure of the amorphous carbon anode as single carbon layer with 6x6 hexagonal rings with functionalized impurity in the form of oxygen compounds. Then we observe how Lithium and Sodium ions after intercalation into the anode will chemically

interact in the presence of these impurities. These calculations were done on Lonestar5 supercomputer at Texas Advanced Computing Center.

Equilibrium geometries of various conformers of carbon monolayer (Fig. 5.1), carbon monolayer with carboxyl group (CM-COOH) (Fig. 5.2 a) and carbon monolayer with hydroxyl group (CM-OH) (Fig. 5.3 a)were optimized. In optimization of electronic structures, the atoms are adjusted such that they obtain the least possible energy structure or equilibrium structures. The base conformer structures were optimized with alkali metal at least 3 Å away from any conformer atom. As shown in the images in the table, after optimization alkali metal directly bonds with the oxygen in the functional compounds in most cases. The only exceptional case of CM-OH/Na where Na bonds with the carbon atom activated by the functional group, hence bonding indirectly to the functional group.

Our synthesized carbon material is amorphous in nature as established by the XRD analysis and hence will be non-graphitic. There has been a lot of studies done on the alkali metal intercalation compounds formed in graphite and non-graphitic carbon [38] so we won't be getting into it. We have done our simulations on an isolated suspended monolayer carbon to prove the alkali metal ion's affinity towards the functionalizing oxygen-based groups. We could have used any carbon structure in principle to make this point but monolayer was chosen for the purpose of reducing computational time and resources.

Our aim was to show that the ions would stagnate into the anode due to their reaction with the functional compounds. This would further decrease the capacity of the battery after the loss due to the formation of Solid Electrolyte Interphase (SEI) after first cycle. A passivation layer called the solid electrolyte interphase is formed on anode surfaces from decomposition products of electrolytes. The SEI allows Li^+ transport and blocks electrons

in order to prevent further electrolyte decomposition and ensure continued electrochemical reactions. Hence SEI is significant for proper battery functioning but also reason for battery degradation due to thickening of this layer more than nanometer scale. This layer and impurities in the anode result in the loss of metal ions and reduction of overall capacity of the battery. The formation and growth mechanism of the nanometer thick SEI films are yet to be completely understood owing to their complex structure and lack of reliable in situ experimental techniques [39]. Meanwhile we can address the impure anode factor. Hence, a synthesis method for anode should be adopted with least possible presence of oxygen based impurities in the product to avoid the additional loss of ions after the first cycle due to ion stagnation.

5.4 Results and Discussion: DFT Interpretation

The geometric and electronic structures and properties of carbon monolayers with 6x6 hexagonal rings in pristine (Fig 5.1.), functionalized and their combination with alkali metal ions (Fig. 5.2 c & Fig. 5.3 c) were compared. The bond lengths in the functionalized carbon were only slightly modified as compared to the pristine carbon. The pristine carbon structure was obtained to be planar after optimization as clearly shown by a lateral view in Figure 5.1 (a). When pristine carbon layer is bonded with a carboxyl or hydroxyl group, we can see in the lateral view of the Figure 5.2 (a) and Figure 5.3 (a) that the planarity of the initial structure is disturbed. The local distortion occurred near the site of adsorption and prominently at the carbon atom connected with the functionalizing groups. Due to this distortion, C-C bond length which is 1.42 Å for sp2 hybridization is stretched up to 1.52Å which is close to C-C bond length of sp3

hybridization. Such a transformation can significantly affect the electronic structure and the resulting properties as discussed further.

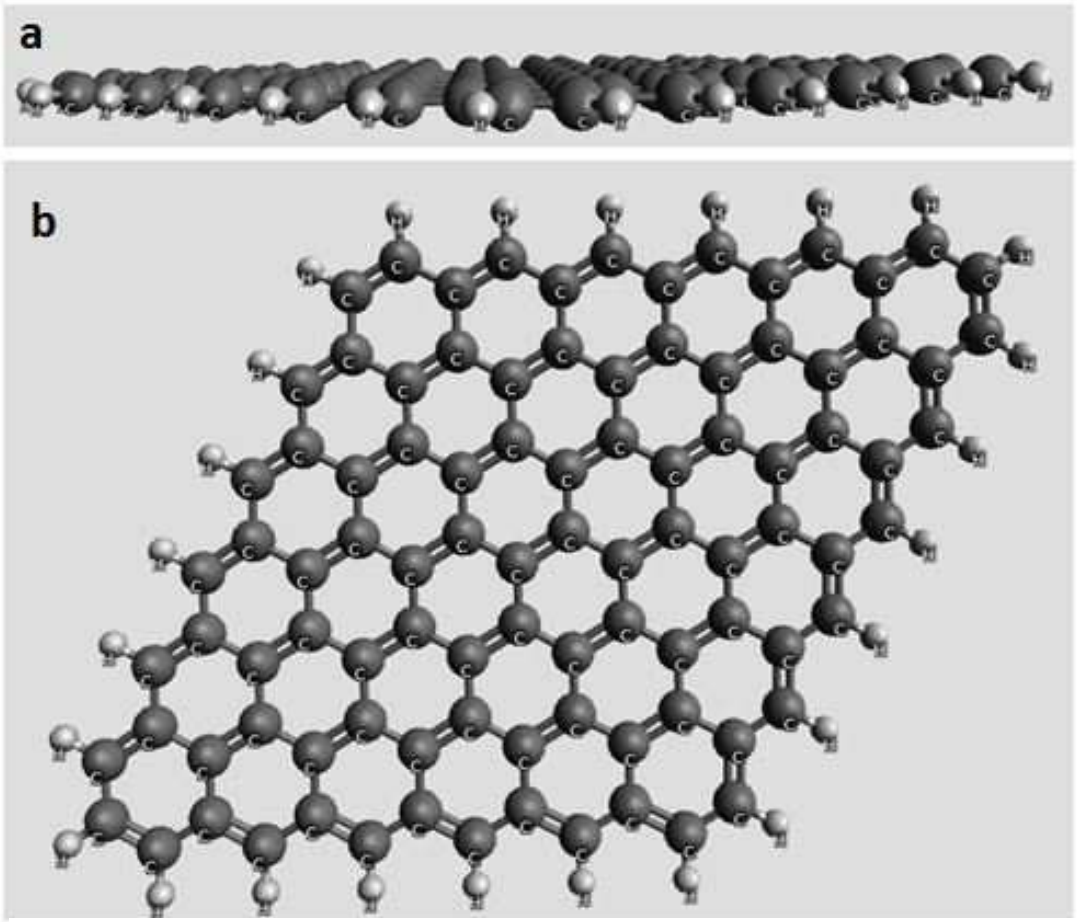

Figure 5.1 The pristine carbon monolayer a) Side view and b) Top view.

The spatial distribution of electrons in the atom is defined by atomic orbitals, whereas the linear combination of atomic orbitals (LCAO) produces the molecular orbitals. The highest occupied molecular orbital (HOMO) and the lowest unoccupied molecular orbital (LUMO) are known as a frontier molecular orbitals. The difference between HOMO and LUMO energies, so-called HOMO–LUMO Gap is an important stability index. This gap for pristine, CM/COOH and CM/OH is 270 meV, 278 meV and 302 meV. Since the HOMO-LUMO gap is more for functionalized carbon structures, they are more stable than the pristine carbon

form. This means that pristine carbon is more potentially favourable to have these functionalized groups in ambient conditions. Though the gap values when compared to ref [40] are different but they follow the same trend. The reason behind the difference in gap values can be attributed to the difference in the basic carbon structures studied. E.V. Rokhina et al in [40] have used a used an effective square ring, while we have a unit cell expanded into super cell of graphene which should be and evidently is more stable.

After establishing base calculations, we have optimized the structure with alkali metals (Li/Na) to its ground state energy. In Fig. 5.2 (b) and (d), Li/Na ions were placed 3Å away from the carboxyl group in the beginning of the calculations. The final configuration achieved after optimization for carboxyl functionalized carbon layer or CM/COOH is shown in Figure 5.2 (c) and Fig. 5.2(e). The Alkali metal ions were attached to the oxygen present in the carboxyl group as we expected. The bond lengths between Li-O was optimized to 1.8 Å and C-C bond length of the distorted carbon was reduced from 1.63 Å to 1.58 Å making the bonding between them stronger. Similarly, for Na-O bond length was optimized to 2.1 Å while C-C bond lengths not changing much.

Though in hydroxyl functionalized carbon layer or CM/OH after optimization in presence of alkali metal ions, it was observed in Fig. 5.3 (c) that hydroxyl group was detached by the Li ion forming Li-OH. Also in Fig. 5.3 (e), sodium ion formed bonds with the distorted carbon rather than forming Na-OH as done by Lithium ion. This could be due to the fact that the Li-OH (427 kJ/mol) have more bond dissociation energy than Na-OH (381 kj/mol) as compared to C-O bond (358 kj/mol: but ideally it should be between 380-420 kJ/mol). However, the final optimized structures being both alkali metal ions bonding with the hydroxyl

group or with bonded atoms connected to hydroxyl group means that the presence of hydroxyl group will attract the ions to interact with it rather than the carbon layer leading to ion stagnation.

Comparing the HOMO-LUMO gap of pristine carbon with alkali metal (pristine/alkali metal) and functionalized carbon with alkali metal will help us make our final point. The gap of pristine/ Na after optimization is 165 meV, which is quite less than the gap observed for CM-COOH/Na i.e. 188 meV and CM-OH/Na i.e. 270.4 meV with Na. Since the energy of functionalized carbon with Na attached to the oxygen impurity or activated carbon due to the functionalized impurity is more, it'll be more stable than just pristine carbon attached to Na ion.

When a battery is charged, the ions from cathode come towards negative anode, gain an electron supplied from the charging source and becomes immobile by making interstitial bonding with the anode. This bonding between anode and reduced metal ion is temporarily stable because metal cannot oxidize by loosing electron and flow around since medium is non-conducting for electrons. Hence this bonding has to wait for an external load to be connected to which electron can flow and reverse the temporary bonding between metal and anode atoms. Carbon-Alkali metal bonding has a small bonding potential with the metal and is able to reverse this bonding but the Oxygen readily oxidize alkali metal ions with high bond potential and makes the bonding very difficult to reverse as shown by our data.

We also calculated the HOMO-LUMO gap of pristine/ Li which was found to be 1.064eV. This value is very large as compared to the CM-COOH/Li i.e. 187 meV and CM-OH/Li i.e. 280 meV. The 5 times higher energy gap of the pristine carbon/Li^+ configuration implies that it is going to be 5 times more stable than Li^+ ion with any functionalized carbon.

Formation energy comparison

Electronic structure formation energy is a measure of energy required to make that system and determine structure's stability. Lower this energy requirement higher the stability. Formation energy of Pristine/Li was obtained to be 18.2 eV which is very large as compared to CM-COOH/Li value 1.03 eV and CM-OH/Li value of 0.32 eV. Hence once Li is bonded with the functionalized groups it'll be very difficult to reverse this reaction.

For the case of Pristine/Na, formation energy was obtained to be 18.3 eV as compared to CM-COOH/Na value of 2.6 eV. Following the above mentioned trend of exception, CM-OH/Na formation energy was found to be 3.4 eV more than the pristine/Na formation energy, making it less stable. Reason for this is not clear. However the overall comparison of formation energy of structures suggest that the oxygen-based functionalization groups/alkali metal structures are much more stable than the pristine configurations. This suggests that alkali metal (and ions) once intercalated in anode during charging will be irreversibly bonded to the oxygen impurities in these groups and will be lost from the net charge capacity.

This concludes that our estimation of stagnation of alkali metal ions is true for sodium and lithium. Hence once attached to these oxygen based functionalized impurities, alkali metal will stagnate there and won't participate in charge-discharge cycles leading to loss of charge capacity. This concludes that the presence of these oxygen based impurities in carbon makes it inadequate for anode application in batteries.

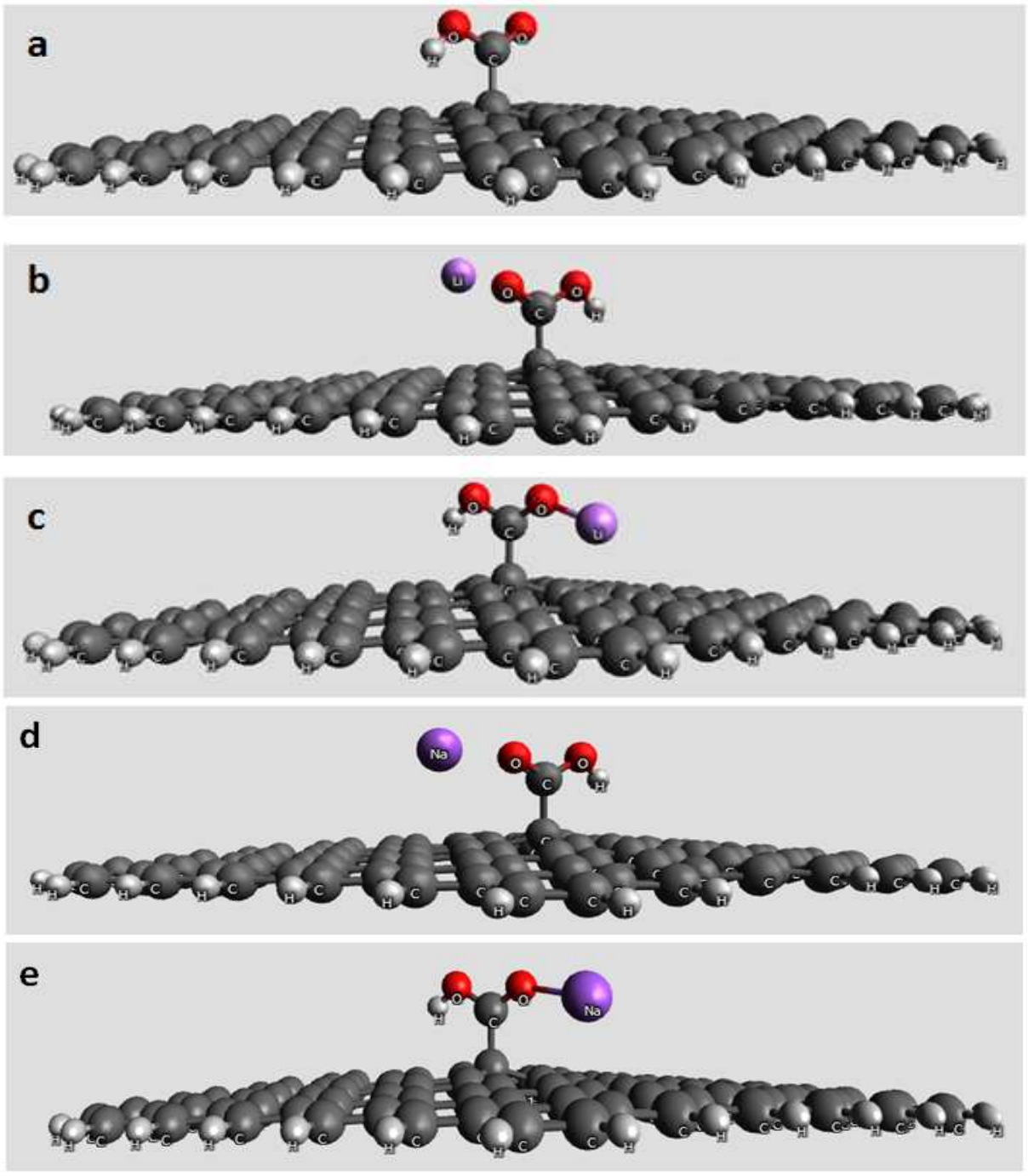

Figure 5.2 Alkali Metal's Chemical affinity to the oxygen based functionalized compound in pristine carbon monolayer, a) carboxyl group functionalized pristine carbon layer, b) Intercalated Li ion in vicinity, c) Li ion getting stagnated by reaction with the oxygen based functionalized group (carboxyl group), d) Intercalated Na ion in vicinity and d) Na ion getting stagnated by reaction with the carboxyl group.

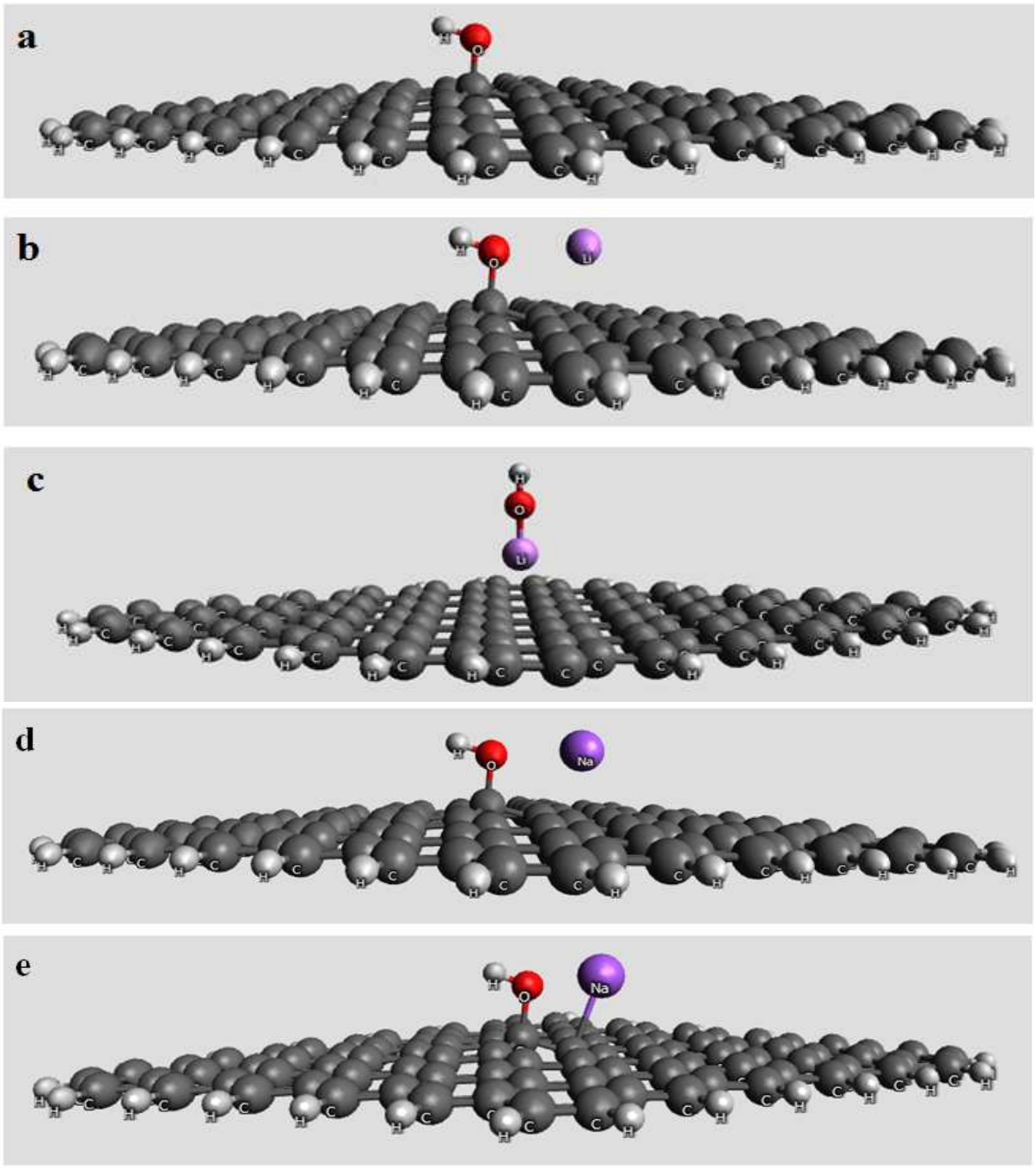

Figure 5.3 Alkali Metal's chemical affinity in the presence of hydroxyl functionalized compound in pristine carbon monolayer, a) hydroxyl group functionalized pristine carbon layer, b) Intercalated Li ion in vicinity, c) Post optimization Li ion displacing hydroxyl group from the monolayer and forming LiOH, d) Intercalated Na ion on the layer and e) Post optimization Na ion reacting with carbon.

CHAPTER VI

CONCLUSION

A carbon foam like material was synthesized with an ease in 3minutes using household microwave oven with $NaCO_3$ particles uniformly ingrained in it. The precursor used were only sugar and baking soda which are household items and are environmentally friendly. Further synthesis was done to decompose the ingrained carbonate to inflate the structure further by release of CO_2 gas. The obtained material was analyzed by XRD, EDS, FESEM and FTIR. XRD showed the progress of the process as intended at each step, EDS concluded the purity of the sample and gave the quantitative idea of composition. FTIR absorbance spectra helped reveal the oxygen based chemical groups present and helped deduce that most of the oxygen impurity, which is reason for ion accumulation in battery electrodes, is trapped as sodium complex. It also supported our claim to state our material suitable for Na ion energy storage electrode. Density Functional Theory simulations were done to show the stagnation of alkali metal in the functionalized carbon materials with carboxyl and hydroxyl groups. After optimization calculation of energies of functionalized carbon in the presence of Li/Na, it was shown in most cases that Li/Na ion will create bonds with the functionalized groups. These bonds are shown to be irreversible by formation energy and HOMO-LUMO gap comparison and hence will be the reason why Li/Na will remain stagnated in the anode. The high surface area morphology observed in FESEM analysis strongly projects our material for energy storage purposes. The fast

and facile synthesis process with environment friendly precursors makes it ideal for large scale eco-friendly production for Na^+ batteries/supercapacitors.

REFERENCES

1. B. L. Ellis and L. F. Nazar, "Sodium and sodium-ion energy storage batteries," *Current Opinion in Solid State and Materials Science*, vol. 16, no. 4, pp. 168–177, 2012.
2. J.-M. Tarascon and M. Armand, "Issues and challenges facing rechargeable lithium batteries," *Nature*, vol. 414, no. 6861, pp. 359–367, 2001.
3. V. Etacheri, R. Marom, R. Elazari, G. Salitra, and D. Aurbach, "Challenges in the development of advanced Li-ion batteries: a review," *Energy & Environmental Science*, vol. 4, no. 9, p. 3243, 2011.
4. A. Yaksic and J. E. Tilton, "Using the cumulative availability curve to assess the threat of mineral depletion: The case of lithium," *Resources Policy*, vol. 34, no. 4, pp. 185–194, 2009..
5. L. Sun, X. Wang, Y. Wang, and Q. Zhang, "Roles of carbon nanotubes in novel energy storage devices," *Carbon*, vol. 122, pp. 462–474, 2017.
6. S. Kumar, Sarita, M. Nehra, N. Dilbaghi, K. Tankeshwar, and K.-H. Kim, "Recent advances and remaining challenges for polymeric nanocomposites in healthcare applications," *Progress in Polymer Science*, vol. 80, pp. 1–38, 2018.
7. E. Frackowiak and F. Béguin, "Carbon materials for the electrochemical storage of energy in capacitors," *Carbon*, vol. 39, no. 6, pp. 937–950, 2001.
8. L. Ji, M. Rao, H. Zheng, L. Zhang, Y. Li, W. Duan, J. Guo, E. J. Cairns, and Y. Zhang, "Graphene Oxide as a Sulfur Immobilizer in High Performance Lithium/Sulfur

Cells," *Journal of the American Chemical Society*, vol. 133, no. 46, pp. 18522–18525, 2011.

9. N. Li, M. Zheng, H. Lu, Z. Hu, C. Shen, X. Chang, G. Ji, J. Cao, and Y. Shi, "High-rate lithium–sulfur batteries promoted by reduced graphene oxide coating," *Chemical Communications*, vol. 48, no. 34, p. 4106, 2012.
10. Y. Huang, X. Dong, Y. Shi, C. M. Li, L.-J. Li, and P. Chen, "Nanoelectronic biosensors based on CVD grown graphene," *Nanoscale*, vol. 2, no. 8, p. 1485, 2010.
11. K. Hata, "Water-Assisted Highly Efficient Synthesis of Impurity-Free Single-Walled Carbon Nanotubes," *Science*, vol. 306, no. 5700, pp. 1362–1364, 2004.
12. A. Reina, X. Jia, J. Ho, D. Nezich, H. Son, V. Bulovic, M. S. Dresselhaus, and J. Kong, "Large Area, Few-Layer Graphene Films on Arbitrary Substrates by Chemical Vapor Deposition," *Nano Letters*, vol. 9, no. 1, pp. 30–35, 2009.
13. X. Ji, K. T. Lee, and L. F. Nazar, "A highly ordered nanostructured carbon–sulphur cathode for lithium–sulphur batteries," *Nature Materials*, vol. 8, no. 6, pp. 500–506, 2009.
14. M. Oschatz, S. Thieme, L. Borchardt, M. R. Lohe, T. Biemelt, J. Brückner, H. Althues, and S. Kaskel, "A new route for the preparation of mesoporous carbon materials with high performance in lithium–sulphur battery cathodes," *Chemical Communications*, vol. 49, no. 52, p. 5832, 2013.
15. S. Thieme, J. Brückner, I. Bauer, M. Oschatz, L. Borchardt, H. Althues, and S. Kaskel, "High capacity micro-mesoporous carbon–sulfur nanocomposite cathodes with enhanced cycling stability prepared by a solvent-free procedure," *Journal of Materials Chemistry A*, vol. 1, no. 32, p. 9225, 2013.
16. N. Jayaprakash, J. Shen, S. S. Moganty, A. Corona, and L. A. Archer, "Porous Hollow Carbon@Sulfur Composites for High-Power Lithium-Sulfur Batteries," *Angewandte Chemie*,

vol. 123, no. 26, pp. 6026–6030, 2011.

17. G. He, S. Evers, X. Liang, M. Cuisinier, A. Garsuch, and L. F. Nazar, "Tailoring Porosity in Carbon Nanospheres for Lithium–Sulfur Battery Cathodes," *ACS Nano*, vol. 7, no. 12, pp. 10920–10930, 2013.
18. P. Strubel, S. Thieme, T. Biemelt, A. Helmer, M. Oschatz, J. Brückner, H. Althues, and S. Kaskel, "ZnO Hard Templating for Synthesis of Hierarchical Porous Carbons with Tailored Porosity and High Performance in Lithium-Sulfur Battery," *Advanced Functional Materials*, vol. 25, no. 2, pp. 287–297, 2014.
19. C. Wang, M. J. O'Connell, and C. K. Chan, "Facile One-Pot Synthesis of Highly Porous Carbon Foams for High-Performance Supercapacitors Using Template-Free Direct Pyrolysis," *ACS Applied Materials & Interfaces*, vol. 7, no. 16, pp. 8952–8960, 2015.
20. A. U. H. S. Rana, M. Kang, and H.-S. Kim, "Microwave-assisted Facile and Ultrafast Growth of ZnO Nanostructures and Proposition of Alternative Microwave-assisted Methods to Address Growth Stoppage," *Scientific Reports*, vol. 6, no. 1, 2016.
21. M. T. H. Aunkor, I. M. Mahbubul, R. Saidur, and H. S. C. Metselaar, "Deoxygenation of graphene oxide using household baking soda as a reducing agent: a green approach," *RSC Advances*, vol. 5, no. 86, pp. 70461–70472, 2015.
22. I.-Y. Jeon, M. J. Ju, J. Xu, H.-J. Choi, J.-M. Seo, M.-J. Kim, I. T. Choi, H. M. Kim, J. C. Kim, J.-J. Lee, H. K. Liu, H. K. Kim, S. Dou, L. Dai, and J.-B. Baek, "Fluorine: Edge-Fluorinated Graphene Nanoplatelets as High Performance Electrodes for Dye-Sensitized Solar Cells and Lithium Ion Batteries (Adv. Funct. Mater. 8/2015)," *Advanced Functional Materials*, vol. 25, no. 8, pp. 1328–1328, 2015.
23. P. Guo, H. Song, and X. Chen, "Electrochemical performance of graphene nanosheets as

anode material for lithium-ion batteries," *Electrochemistry Communications*, vol. 11, no. 6, pp. 1320–1324, 2009.

24. G. Wang, X. Shen, J. Yao, and J. Park, "Graphene nanosheets for enhanced lithium storage in lithium ion batteries," *Carbon*, vol. 47, no. 8, pp. 2049–2053, 2009.
25. S. Roberts and E. Kendrick, "The re-emergence of sodium ion batteries: testing, processing, and manufacturability," *Nanotechnology, Science and Applications*, vol. Volume 11, pp. 23–33, 2018.
26. H. Ulbricht, G. Moos, and T. Hertel, "Physisorption of molecular oxygen on single-wall carbon nanotube bundles and graphite," *Physical Review B*, vol. 66, no. 7, May 2002.
27. B. F. Tjeerdsma and H. Militz, "Chemical changes in hydrothermal treated wood: FTIR analysis of combined hydrothermal and dry heat-treated wood," *Holz als Roh- und Werkstoff*, vol. 63, no. 2, pp. 102–111, 2005.
28. K. Krishnamoorthy, M. Veerapandian, K. Yun, and S.-J. Kim, "The chemical and structural analysis of graphene oxide with different degrees of oxidation," *Carbon*, vol. 53, pp. 38–49, 2013.
29. W. Xu, J. Wang, F. Ding, X. Chen, E. Nasybulin, Y. Zhang, and J.-G. Zhang, "Lithium metal anodes for rechargeable batteries," *Energy Environ. Sci.*, vol. 7, no. 2, pp. 513–537, 2014.
30. W. Luo and L. Hu, "Na Metal Anode: 'Holy Grail' for Room-Temperature Na-Ion Batteries?," ACS Central Science, vol. 1, no. 8, pp. 420–422, Dec. 2015.
31. X. Zheng, C. Bommier, W. Luo, L. Jiang, Y. Hao, and Y. Huang, "Sodium metal anodes for room-temperature sodium-ion batteries: Applications, challenges and solutions," *Energy Storage Materials*, vol. 16, pp. 6–23, 2019.
32. M. Nuechter, B. Ondruschka, W. Bonrath, and A. Gum, "Microwave-Assisted Synthesis: A

Critical Technology Overview," *ChemInform*, vol. 35, no. 51, 2004.

33. Y. Y. Xi, Y. F. Hsu, and W. K. Chan, "Hydrothermal Synthesis of Nanostructures," *Recent Patents on Nanotechnology*, vol. 1, no. 2, pp. 121–128, Jan. 2007.
34. E. Chełmecka, K. Pasterny, T. Kupka, and L. Stobiński, "Density functional theory studies of OH-modified open-ended single-wall zigzag carbon nanotubes (SWCNTs)," *Journal of Molecular Structure: THEOCHEM*, vol. 948, no. 1-3, pp. 93–98, 2010.
35. Gaussian 16, Revision C.01, M. J. Frisch, G. W. Trucks, H. B. Schlegel, G. E. Scuseria, M. A. Robb, J. R. Cheeseman, G. Scalmani, V. Barone, G. A. Petersson, H. Nakatsuji, X. Li, M. Caricato, A. V. Marenich, J. Bloino, B. G. Janesko, R. Gomperts, B. Mennucci, H. P. Hratchian, J. V. Ortiz, A. F. Izmaylov, J. L. Sonnenberg, D. Williams-Young, F. Ding, F. Lipparini, F. Egidi, J. Goings, B. Peng, A. Petrone, T. Henderson, D. Ranasinghe, V. G. Zakrzewski, J. Gao, N. Rega, G. Zheng, W. Liang, M. Hada, M. Ehara, K. Toyota, R. Fukuda, J. Hasegawa, M. Ishida, T. Nakajima, Y. Honda, O. Kitao, H. Nakai, T. Vreven, K. Throssell, J. A. Montgomery, Jr., J. E. Peralta, F. Ogliaro, M. J. Bearpark, J. J. Heyd, E. N. Brothers, K. N. Kudin, V. N. Staroverov, T. A. Keith, R. Kobayashi, J. Normand, K. Raghavachari, A. P. Rendell, J. C. Burant, S. S. Iyengar, J. Tomasi, M. Cossi, J. M. Millam, M. Klene, C. Adamo, R. Cammi, J. W. Ochterski, R. L. Martin, K. Morokuma, O. Farkas, J. B. Foresman, and D. J. Fox, Gaussian, Inc., Wallingford CT, 2016.
36. *P. J. Stephens, F. J. Devlin, C. F. Chabalowski, and M. J. Frisch, "Ab Initio Calculation of Vibrational Absorption and Circular Dichroism Spectra Using Density Functional Force Fields," The Journal of Physical Chemistry, vol. 98, no. 45, pp. 11623–11627, 1994.*
37. A. D. Becke, "A new mixing of Hartree–Fock and local density-functional theories," *The*

Journal of Chemical Physics, vol. 98, no. 2, pp. 1372–1377, 1993.

38. J.-X. Huang, G. Csányi, J.-B. Zhao, J. Cheng, and V. L. Deringer, "First-principles study of alkali-metal intercalation in disordered carbon anode materials," *Journal of Materials Chemistry A*, vol. 7, no. 32, pp. 19070–19080, 2019.
39. A. Wang, S. Kadam, H. Li, S. Shi, and Y. Qi, "Review on modeling of the anode solid electrolyte interphase (SEI) for lithium-ion batteries," *npj Computational Materials*, vol. 4, no. 1, 2018.
40. E. V. Rokhina, M. Lahtinen, K. Makarova, V. Jegatheesan, and J. Virkutyte, "Theoretical and practical aspects of chemical functionalization of carbon nanofibers (CNFs): DFT calculations and adsorption study," *Bioresource Technology*, vol. 113, pp. 127–131, 2012.

BIOGRAPHICAL SKETCH

Varun Gupta was born on November 27, 1992. He has done his Bachelor of Sciencehonorsin Physics from University of Delhi 2014. He completed his master's in Physics from Jawaharlal Nehru University, New Delhi, India in May 2017. In his master's in Physics, he did a lot of research in condensed matter physics and published 3 articles. Seeking interest in application based research, he obtained a Master of Science degree in Electrical Engineering from University of Texas Rio Grande Valley, Texas, USA in May 2020.

Address:

905 N Sugar Rd Apt # 1002

Edinburg, Texas, USA, 78541.

His Publications:

1. Tuning electronic and magnetic properties of CuAlO2 nanocrystals using magnetic dopants. N. Ray, V. Gupta, L. Sarma, P. Kush, J. Nag, and S. Sapra ACS Omega, 3 (1), 509-513 (2018).
2. Permeability of two-dimensional Graphene and hexagonal-Boron Nitride sheets to Hydrogen. V. Gupta, A. Kumar and N. Ray Pramana: J. Phys. (2018).
3. Conference publication: Permeability of two-dimensional Graphene and hexagonal-Boron Nitride sheets to Hydrogen atom. V. Gupta, A. Kumar and N. Ray AIP Conference Proceedings 1953, 140013 (2018).